A Parameterized Linear Magnetic Equivalent Circuit for Analysis and Design of Radial Flux Magnetic Gears–Part II: Evaluation

Matthew Johnson, *Member, IEEE*, Matthew C. Gardner, *Student Member, IEEE*, Hamid A. Toliyat, *Fellow, IEEE*

***Abstract*--This is Part II of a two part paper on the development of a parameterized linear magnetic equivalent circuit (MEC) for radial flux magnetic gears with surface permanent magnets. Part I describes the MEC implementation. This section, Part II, evaluates the MEC model's accuracy by comparing its results against those produced by a nonlinear Finite Element Analysis (FEA) model. Simulation results demonstrate that the linearity approximation does not prevent the MEC from accurately matching the torque and air gap flux densities predicted by a nonlinear FEA model for three diverse magnetic gear base designs. The impacts of the MEC discretization parameters introduced in Part I are also investigated using the same base designs, and guidelines for those settings are developed. Additionally, single design parameter sweeps illustrate the MEC's ability to track these changes over most practical design ranges and reveal where the MEC's accuracy degrades due to the linearity approximation. Finally, the results of a 46,656 case parametric optimization study demonstrate the MEC's ability to match the nonlinear FEA model's torque predictions within a few percent over a wide range of designs while achieving average simulation speeds 44 to 271 times faster than those of the FEA model.**

***Index Terms*--finite element analysis, magnetic equivalent circuit, magnetic gear, optimization, permeance network, radial flux, reluctance network, torque density.**

I. Introduction

MAGNETIC gears perform the same fundamental task as mechanical gears, transferring mechanical power between high-torque, low-speed rotation and low-torque, high-speed rotation. However, magnetic gears transfer power through the modulated interaction of magnetic fields, instead of through interlocking teeth. While this contactless operation offers many potential benefits, fast and accurate analysis tools are required to develop high performing application-specific designs capable of achieving commercial success.

The most prevalent electromechanical system analysis tools include finite element analysis (FEA) models, analytical models, winding function theory (WFT), and magnetic equivalent circuit (MEC) models. FEA models are the overwhelmingly most popular choice for analysis of magnetic gears due to their broad commercial availability, ease of use, and high degree of accuracy, including the ability to characterize 3D and nonlinear effects [1], [2]. However, these benefits come at the expense of high computational intensity and long simulation run times. This is a particularly significant issue for magnetic gears, which have different permanent magnet pole counts on the two rotors and an intermediate set of modulators that produce numerous significant spatial harmonics in the field distribution, as well as substantial leakage flux in multiple regions. These issues, combined with the presence of two air gaps, necessitate the use of numerous small mesh elements to accurately determine the field solution. Furthermore, most good designs have limited symmetry to decrease torque ripple [3], which mitigates the usefulness of faster fractional models.

Alternatively, analytical models have also been developed for certain magnetic gear topologies. While these tools can be much faster than FEA models, they are relatively topology specific and inflexible. Furthermore, they are typically based on simplifying assumptions and either severely limited or completely lacking in ability to accurately model 3D effects and nonlinear effects, such as iron saturation, without introducing significant complications [4], [5]. Similarly, a WFT model has also demonstrated reasonably accurate results for a single design case [6]. However, its underlying assumptions prevent it from correctly characterizing the complex flux paths present in many magnetic gear designs. Therefore, analytical and WFT models are not ideally suited for extensive magnetic gear optimization studies. MECs, also referred to as reluctance networks, are an alternative tool that represents a compromise between the accuracy and flexibility of FEA models and the speed of analytical models.

This is Part II of a two part paper on the development of a parameterized linear 2D MEC for radial flux magnetic gears with surface permanent magnets, as shown in Fig. 1 of Part I. Part I describes the systematic implementation of the MEC, including the formation of the reluctance network, the construction of the system permeance matrix, and the solution of the resulting system of equations. As noted in Part I, this

M. Johnson is with the Advanced Electric Machines and Power Electronics Lab in the Department of Electrical and Computer Engineering at Texas A&M University, College Station, TX 77843 USA (e-mail: mjohnson11@tamu.edu).

M. C. Gardner is with the Advanced Electric Machines and Power Electronics Lab in the Department of Electrical and Computer Engineering at Texas A&M University, College Station, TX 77843 USA (e-mail: gardner1100@tamu.edu).

H. A. Toliyat is with the Advanced Electric Machines and Power Electronics Lab in the Department of Electrical and Computer Engineering at Texas A&M University, College Station, TX 77843 USA (e-mail: toliyat@tamu.edu).

implementation can be easily extended to create 3D or nonlinear models, and those developments will be presented in future papers. This section, Part II, provides a detailed evaluation of the MEC model's performance by comparing its torque and flux density predictions with those of a non-linear FEA model constructed in ANSYS Maxwell. Three diverse magnetic gear base designs are used throughout several of the different comparison studies, and an extensive parametric design optimization study serves as the final test to assess the MEC's utility for analyzing a wide range of different designs.

II. Impact of Linearity Assumption

The radial flux magnetic gear 2D MEC model implementation presented in Part I introduced the fundamental simplifying assumption of fixed permeability *B-H* characteristics in the modulators and rotor back irons, as well as 8 different independent discretization parameters: the number of angular layers (N_{AL}) and the numbers of radial layers in the high speed rotor (HSR) back iron, the HSR magnets, the HSR air gap, the modulators, the low speed rotor (LSR) air gap, the LSR magnets, and the LSR back iron ($N_{RL,HSBI}$, $N_{RL,HSPM}$, $N_{RL,HSAG}$, $N_{RL,Mods}$, $N_{RL,LSAG}$, $N_{RL,LSPM}$, and $N_{RL,LSBI}$, respectively). Before deploying the MEC model, it is critical to evaluate its accuracy and characterize the impact of the linearity assumption and various mesh discretization parameters on that accuracy. This step is neglected in many MEC studies which rely on a fixed, coarse lumped element distribution as opposed to a fully parameterized network of elements [7]-[9]. Table I summarizes the three different magnetic gear "base designs" selected for use in this analysis. Fig. 1 shows cross-sections of the same base designs. All gear designs evaluated in this study use NdFeB N42 magnets and M47 electrical steel for the modulators and back irons. Note that G_r represents the integer part of the desired gear ratio, assuming that the modulators are fixed and the inner permanent magnet high speed rotor (HSR) and outer permanent magnet low speed rotor (LSR) rotate. G_r and the HSR permanent magnet pole pair count (P_{HS}) determine the LSR permanent magnet pole pair count (P_{LS}), according to

$$P_{LS} = \begin{cases} G_r P_{HS} + 1 & \text{for } (G_r + 1)P_{HS} \text{ odd} \\ G_r P_{HS} + 2 & \text{for } (G_r + 1)P_{HS} \text{ even} \end{cases}. \quad (1)$$

This approach keeps the number of modulators (Q_M) even, which symmetrically cancels the net forces on each rotor, and maintains a relatively high least common multiple between P_{HS} and P_{LS}, which reduces the gear's torque ripple [1], [3]. In particular, this approach avoids integer gear ratios, which suffer from significant torque ripple. In addition to the parameters specified in Table I, 100% angular fill factors were used for each magnet pole in all base designs. All modulators used 50% angular fill factors, resulting in equally distributed modulator pieces and slots. Although limited in quantity, these designs were specifically chosen to provide a relatively diverse sampling of somewhat reasonable gear configurations with varying parameter values to avoid biasing the results. The base designs are also chosen to avoid excessive saturation; however, they are not intended to be optimal.

TABLE I
Magnetic Gear Base Designs for MEC Model Evaluation

Parameter	Description	Base Design 1	Base Design 2	Base Design 3	Units
G_r	Integer part of gear ratio	4	8	16	
P_{HS}	HSR pole pairs	11	4	6	
r_{out}	Gear active outer radius	150	175	200	mm
T_{HSBI}	HSR back iron thickness	20	35	40	mm
T_{HSPM}	HSR magnet thickness	9	5	13	mm
T_{HSAG}	HSR air gap thickness	0.5	2	1	mm
T_{Mods}	Modulator thickness	11	17	14	mm
T_{LSAG}	LSR air gap thickness	0.5	2	1	mm
T_{LSPM}	LSR magnet thickness	7	5	7	mm
T_{LSBI}	LSR back iron thickness	20	30	25	mm

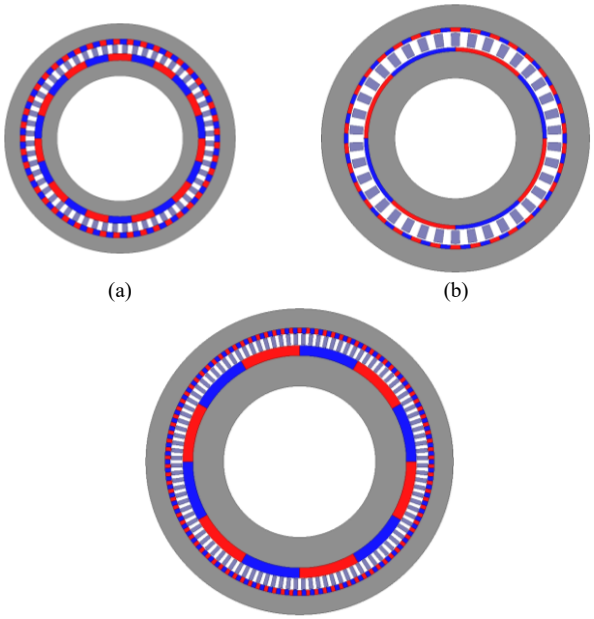

Fig. 1. Cross-sectional views of base designs (a) 1, (b) 2, and (c) 3.

First, the impact of the linear ferromagnetic material assumption was evaluated by sweeping the constant relative permeability of the material used in both the rotor back irons and the modulators from 10 to 4000 and evaluating the resulting LSR stall torque predicted by the MEC model at each permeability for all three of the base designs. Unless otherwise specified, all results are based on the LSR stall torque; alternatively, the modulator assembly stall torque could be used, and the trends would be identical with proportionally higher torque and torque density values. Each simulation case in the permeability sweep was evaluated using the same extremely tight (and extremely inefficient) mesh for all base designs, with 4000 angular layers and 30 radial layers in each of the 7 radial regions. The results of the permeability sweep study are illustrated in Fig. 2, which shows the variation in the accuracy of the stall torque predicted by the MEC model at each constant permeability setting relative to that predicted for the corresponding base design by an ANSYS Maxwell FEA model using nonlinear M47 steel *B-H* characteristics for the modulators and rotor back irons.

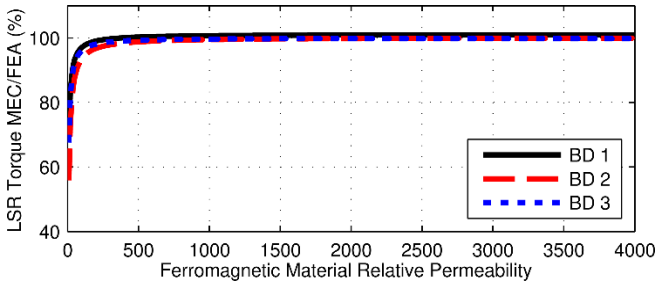

Fig. 2. Impact of linear ferromagnetic material relative permeability on the MEC model accuracy for each base design (BD).

The points depicted in Fig. 2 indicate two key results. First, the approximation of linearity is valid for the three base designs and, as long as the assumed relative permeability of the ferromagnetic material is above a certain minimum setting (in this case, approximately 500), it has little impact on the MEC model torque predictions. As previously suggested, this is true because the linear reluctances of the permanent magnets and air gaps dwarf the non-linear reluctances of the back irons and modulators for most practical ideal designs. Consequently, for all following MEC model studies, the relative permeability of the ferromagnetic material was set to 3000, which is the approximate relative permeability of M47 up to its knee point. The results in Fig. 2 also indicate that the MEC model is extremely accurate based on the selected settings for the three base designs, asymptotically approaching torque prediction errors of 1%, -0.05%, and -0.2% for each of these designs. These accuracies are well within the margins of error for FEA modeling tools and the uncertainty resulting from realistic manufacturing practices.

III. Impact of Discretization Settings

Each discretization parameter provides a tradeoff between higher accuracy with more elements and reduced simulation time and memory with fewer elements. In order to evaluate the impact of the number of angular layers on the MEC model's accuracy, N_{AL} was swept from 50 to 6000 in steps of 25 and the MEC model torque prediction was evaluated at each setting for each base design, as illustrated in Fig. 3. Each simulation case used a relatively tight mesh of 18 radial layers in each of the gear's 7 radial regions. These results again indicate that the MEC model converges to a very accurate torque prediction for each of the three base designs, asymptotically approaching percent errors of 1%, 0.2%, and 0.7% relative to the corresponding FEA predictions.

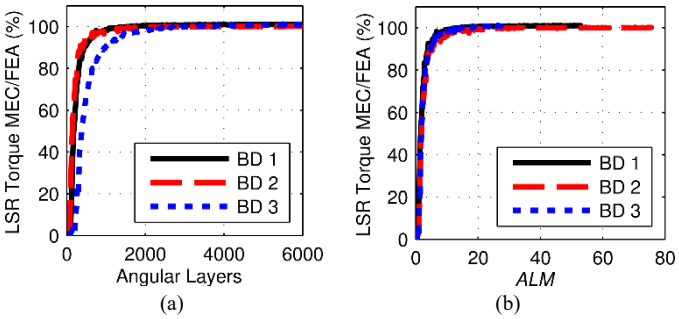

Fig. 3. Variation of MEC model accuracy with (a) the number of angular layers and (b) the angular layers multiplier (*ALM*) for each base design (BD).

The results in Fig. 3(a) also illustrate that the MEC model torque predictions increase as the number of angular layers increases. A much wider set of designs was evaluated during the model development, and this pattern remained true in every case. In general, the variations of the MEC's torque predictions stem from how accurately the discretization settings capture the harmonic field content and leakage flux distribution for each design.

Unfortunately, the results in Fig. 3(a) also indicate that the torque predictions for the different designs converge to the correct values at significantly different numbers of angular layers. While using a large constant number of angular layers for all designs would provide high accuracy, it would also result in excessive angular layer counts and unnecessarily slower simulation run times for many designs. Instead, this study sets the angular layer count based on the number of modulators in each design by using the angular layers multiplier (*ALM*), defined as

$$ALM = N_{AL}/(2Q_M) \tag{2}$$

which is the number of angular layers for each modulator or slot. This approach was selected because the modulators are the features with the smallest tangential width in any design. Fig. 3(b) shows the same information as Fig. 3(a), but the horizontal axis indicates the *ALM* value for each point instead of the number of angular layers. This graph demonstrates that the MEC model torque predictions for all three base designs converge to the correct values at approximately the same rate with respect to *ALM* values, which is the desired effect. During the MEC model development, this trend was evaluated over a larger design set and proved to be very consistent, although there is some small variation in the necessary *ALM* based on other features besides the number of modulators.

In order to evaluate the relative impacts of the number of radial layers in each radial region, each of these 7 discretization parameters was independently swept from 1 to 40 radial layers while all other radial layer parameters were each fixed at 12 radial layers. An angular layers multiplier of 20 was used for each simulation case. The results for all radial layer parameters are shown for each base design in Fig. 4.

The different curves in Fig. 4 correspond to the radial layer discretization parameters and the horizontal axis indicates the number of radial layers used in the specified radial region. For all three designs, the number of radial layers in the LSR magnets and the modulators are the most critical parameters. Additionally, the number of HSR PM layers can also have a small impact for some designs. The number of radial layers in either air gap has an extremely limited impact, and the number of layers in either back iron region has essentially no impact, which is not surprising given the trends in Fig. 2. As a result, the four corresponding curves are all nearly horizontal in each graph. While all of the results shown in Fig. 4 indicate that increasing the number of radial layers decreases the model's torque predictions, likely due to more accurate leakage flux characterizations, increasing the number of radial layers in certain regions, such as the modulators, actually slightly increases the torque prediction for a few designs.

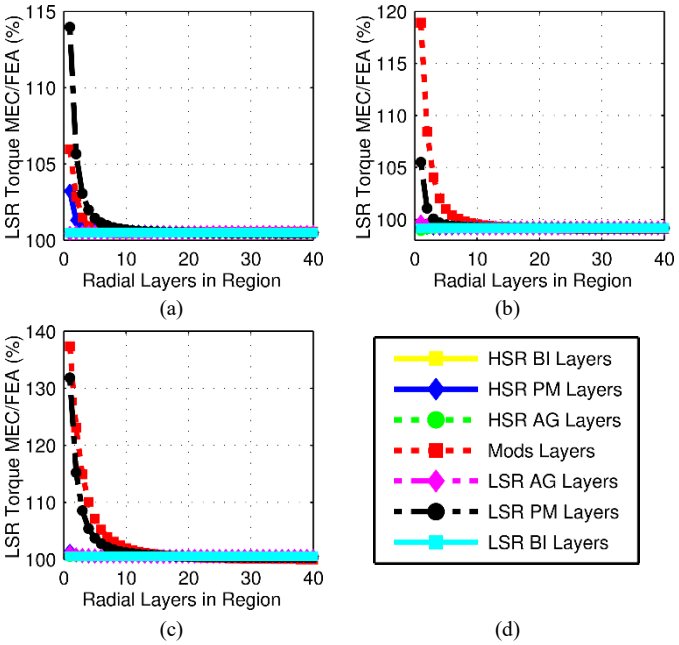

Fig. 4. Variation of MEC model accuracy for base designs (a) 1, (b) 2, and (c) 3 with the radial layer counts in (d) each radial region.

The results in Fig. 4 also demonstrate that the torque predictions converge to the correct answers at different radial layer counts, as with the angular layer counts. Fig. 5(a) shows the impact of the LSR permanent magnet radial layers on the MEC torque prediction for the base designs to further highlight these differences. Note that the torque values for each point in any one curve are normalized by the torque value associated with the last point in that curve to appropriately scale the graph and determine the values at which further increasing the number of radial layers ceases to significantly change the model's torque predictions. To eliminate the issue of these differing convergence rates, the LSR permanent magnet radial layers multiplier, RLM_{LSPM}, defined as

$$RLM_{LSPM} = \frac{(\pi r_{LSPM}/P_{LS})}{(T_{LSPM}/N_{RL,LSPM})} \tag{3}$$

where r_{LSPM} is the radius in the middle of the LSR permanent magnets, was developed to select the radial layer count in the LSR permanent magnet region based on the pole arc and radial thickness of the magnets. Decreasing the LSR magnet pole arc and increasing the LSR magnet thickness both tend to increase the leakage flux in this area, which necessitates the use of more radial layers in this region to accurately characterize the field solution. Using (3) with a fixed RLM_{LSPM} value achieves this desired effect. Fig. 5(b) shows the same information as Fig. 5(a), but the horizontal axis indicates the LSR permanent magnet radial layers multiplier value for each point instead of the number of LSR permanent magnet radial layers. This graph demonstrates that the MEC torque predictions for all three base designs converge to the correct values at approximately the same rate with respect to LSR permanent magnet radial layers multiplier values, which is the desired effect. This trend proved to be very consistent over a larger design set during the MEC model development.

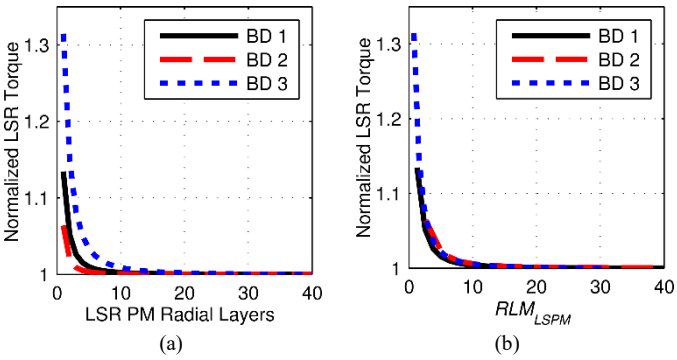

Fig. 5. Variation of the MEC model LSR torque prediction with (a) the number of LSR PM radial layers and (b) the LSR PM radial layers multiplier (RLM_{LSPM}) for each base design (BD).

A modulators radial layers multiplier, RLM_{Mods}, and an HSR permanent magnet radial layers multiplier, RLM_{HSPM}, are also similarly defined for their respective regions as

$$RLM_{Mods} = \frac{(\pi r_{Mods}/Q_M)}{(T_{Mods}/N_{RL,Mods})} \tag{4}$$

$$RLM_{HSPM} = \frac{(\pi r_{HSPM}/P_{HS})}{(T_{HSPM}/N_{RL,HSPM})} \tag{5}$$

where r_{Mods} and r_{HSPM} are the radii in the middles of the modulators and of the LSR permanent magnets, respectively. While the torque predictions do not converge at the same values of RLM_{Mods} quite as nicely as with the RLM_{LSPM}, using the RLM_{Mods} provides a significant improvement over a fixed number of radial layers in the modulators. Although the number of radial layers used in the HSR permanent magnet region does not have as large of an effect on the MEC model's torque predictions as the number of layers in the LSR permanent magnets and the modulators, the RLM_{HSPM} does provide an effective means of uniformly controlling this torque prediction convergence across the different designs. Despite the extremely limited impact of the number of radial layers in the air gaps, an HSR air gap radial layers multiplier, RLM_{HSAG}, and an LSR air gap radial layers multiplier, RLM_{LSAG}, are also defined as

$$RLM_{HSAG} = \frac{(\pi r_{HSAG}/P_{HS})}{(T_{HSAG}/N_{RL,HSAG})} \tag{6}$$

$$RLM_{LSAG} = \frac{(\pi r_{LSAG}/P_{LS})}{(T_{LSAG}/N_{RL,LSAG})} \tag{7}$$

where r_{HSAG} and r_{LSAG} are the radii in the middles of the high speed and low speed air gaps, respectively. Because the radial layer counts in the back irons have negligible impact on the torque predicted by the MEC model for most designs, small fixed radial layer counts are used in these regions.

IV. Single Parameter Sweeps

In order to further demonstrate the accuracy of the MEC model and to illustrate scenarios in which the linearity assumption introduces significant error, the three base designs

previously specified in Table I were used as starting points and the individual design parameters included in Table II were independently swept over the ranges of values specified in Table II. For example, all other parameters specified in Table I were fixed while P_{HS} was swept from 3 to 15 in each base design. Each of the resulting design points was evaluated using a 2D MEC model with the "fine mesh" discretization settings specified in Table III and a nonlinear 2D FEA model.

Fig. 6 depicts the variation of the MEC accuracy with the HSR back iron thickness, LSR back iron thickness, modulator thickness, and modulator angular fill factor. For each of these parameters, the MEC is extremely accurate over most of the range of considered values; however, when any of the component dimensions becomes sufficiently thin, the ferromagnetic material becomes heavily saturated, causing the assumption of linearity to break down and the MEC to overestimate the torque. It is important to note that most of these parameter values which cause the system to become appreciably nonlinear and the model to become inaccurate are impractically small from a mechanical design and manufacturing standpoint. This is consistent with the linear magnetic gear modulator thickness analysis presented in [10].

TABLE II
Magnetic Gear Base Design Single Parameter Sweeps

Parameter	Description	Ranges of Values	Units
T_{HSBI}	HSR back iron thickness	1, 2, 3, … 40	mm
T_{HSPM}	HSR magnet thickness	1, 2, 3, … 25	mm
T_{HSAG}	HSR air gap thickness	0.25, 0.5, 0.75, … 5	mm
T_{Mods}	Modulator thickness	1, 2, 3, … 20	mm
T_{LSAG}	LSR air gap thickness	0.25, 0.5, 0.75, … 5	mm
T_{LSPM}	LSR magnet thickness	1, 2, 3, … 25	mm
T_{LSBI}	LSR back iron thickness	1, 2, 3, … 30	mm
P_{HS}	HSR pole pairs	3, 4, 5, … 15	
α_{Mods}	Modulators angular fill factor	0.05, 0.1, 0.15, … 0.95	
α_{HSPM}	HSR magnets angular fill factor	0.1, 0.2, 0.3, … 1	
α_{LSPM}	LSR magnets angular fill factor	0.1, 0.2, 0.3, … 1	
r_{out}	Gear active outer radius	125, 130, 135, … 200	mm

TABLE III
Magnetic Gear MEC Model Discretization Settings for the Single Parameter Sweep Study and the Optimization Study

Parameter	Description	Coarse Mesh	Fine Mesh
ALM	Angular layers multiplier	10	30
$N_{RL,HSBI}$	Radial layers in the HSR back iron	3	3
RLM_{HSPM}	HSR magnets radial layers multiplier	10	20
RLM_{HSAG}	HSR air gap radial layers multiplier	10	20
RLM_{Mods}	Modulators radial layers multiplier	10	20
RLM_{LSAG}	LSR air gap radial layers multiplier	10	20
RLM_{LSPM}	LSR magnets radial layers multiplier	10	20
$N_{RL,LSBI}$	Radial layers in the LSR back iron	3	3
$N_{RL,HSPM,min}$	Minimum radial layers in HSR magnets	3	3
$N_{RL,HSAG,min}$	Minimum radial layers in HSR air gap	3	3
$N_{RL,Mods,min}$	Minimum radial layers in modulators	3	5
$N_{RL,LSAG,min}$	Minimum radial layers in LSR air gap	3	3
$N_{RL,LSPM,min}$	Minimum radial layers in LSR magnets	3	5

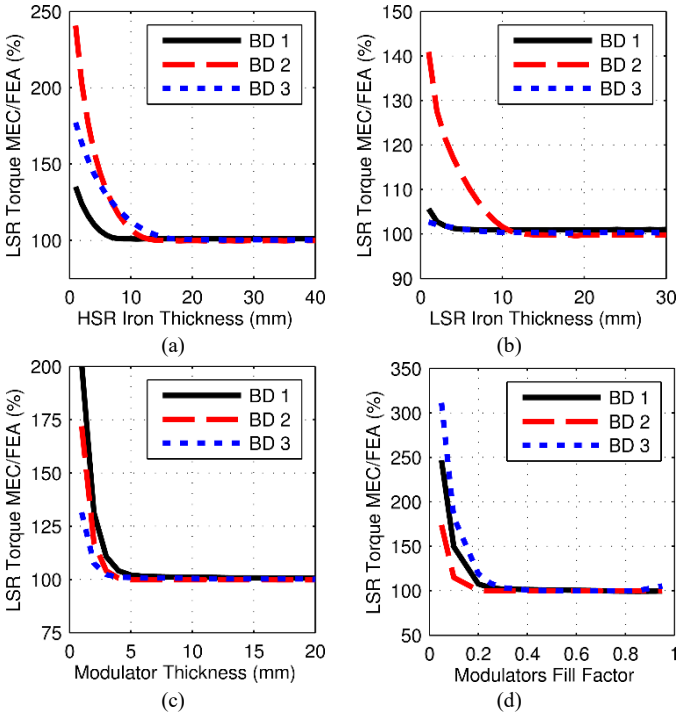

Fig. 6. Variation of MEC accuracy with (a) HSR back iron thickness, (b) LSR back iron thickness, (c) modulator radial thickness and (d) modulator angular fill factor for each base design (BD).

Additionally, variations in the HSR and LSR magnet thicknesses, HSR and LSR magnet angular fill factors, HSR and LSR air gap thicknesses, HSR pole pair count, and outer radius were evaluated for each of the base designs, as described in Table II. The MEC is very accurate over the full range of values considered for these parameters, with at most only a 2.5% variation in accuracy between the extreme ends of the relatively broad parameter value spectrums. These slight fluctuations in accuracy are due to a combination of MEC mesh discretization considerations and the effects of the parameter variations on saturation and magnetic flux leakage. However, the accuracy of the MEC torque predictions would not be as constant with respect to the variation of certain key parameters if a fixed mesh with constant angular and radial layer counts was used instead of the scalable mesh settings specified in Table III.

V. Flux Density Comparisons

The preceding sections evaluated the MEC model based solely on the accuracy of its torque predictions relative to those of the nonlinear FEA model. It is also beneficial to compare the flux density distributions predicted by the two models. Fig. 7 shows the radial flux density distributions predicted by the FEA and MEC models along circular paths in the radial middle of the LSR air gaps for all 3 base designs. These results demonstrate that the MEC also produces very accurate air gap flux density distributions. In fact, for these designs, the flux density distributions are very accurate in all regions, except for the back irons where there are some slight errors at the peak flux density points due to the assumption of linear ferromagnetic material *B-H* characteristics.

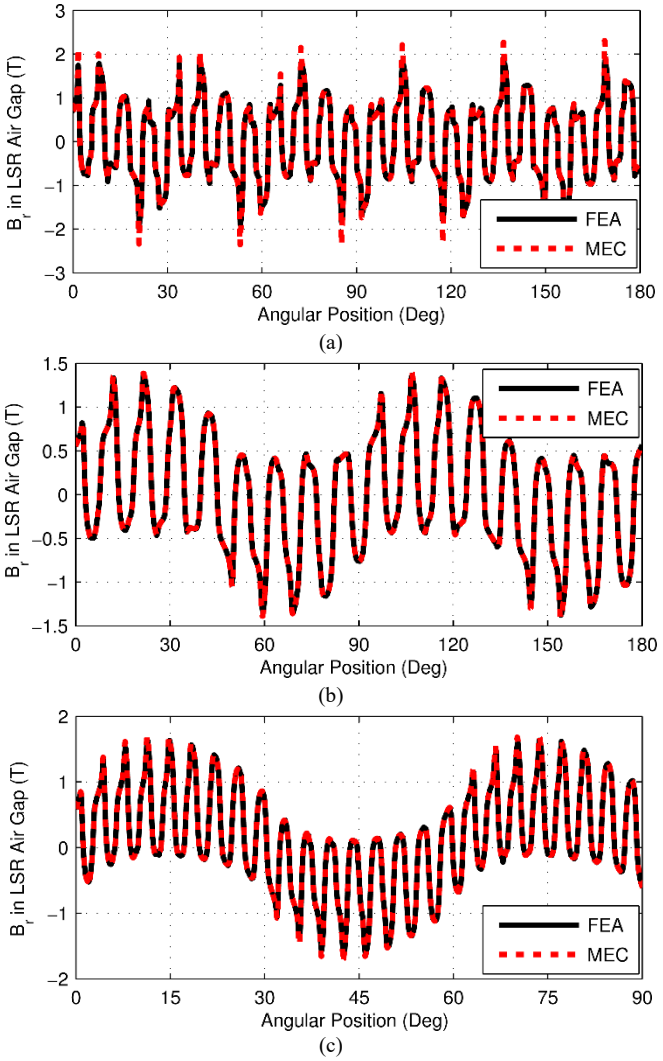

Fig. 7. Radial flux density along a circular path in the radial middle of the LSR air gap of base designs (a) 1, (b) 2, and (c) 3.

VI. Optimization Study

The most important test of the MEC model as a design tool is an example optimization study. As demonstrated by the graphs in the previous sections, saturation or an inadequately low number of radial layers can cause the MEC model to overestimate a design's stall torque, but an inadequately low number of angular layers can cause the MEC model to underestimate the stall torque of the same design. Thus, using insufficient radial and angular layer counts may result in fast models with accurate stall torque predictions for a single design or a small set of designs. However, if such a low resolution model is applied to a broader range of designs, its accuracy will be inconsistent, and this may bias the results towards a certain subset of designs. Therefore, several critical gear parameters were swept over the wide ranges of values specified in Table IV, and each of the resulting 46,656 designs was evaluated using the 2D MEC model with both the "coarse mesh" and the "fine mesh" settings specified in Table III, as well as a 2D nonlinear FEA model. Although the coarse mesh is much looser than the fine mesh, it still results in much higher resolution reluctance networks than most of those used in other MEC studies described in the literature [7]-[9].

TABLE IV
Optimization Study Parameter Sweep Ranges

Parameter	Description	Ranges of Values	Units
G_r	Integer part of gear ratio	4, 8, 16	
P_{HS}	HSR pole pairs		
	For $G_r = 4$	4, 5, 6, … 18	
	For $G_r = 8$	3, 4, 5, … 13	
	For $G_r = 16$	3, 4, 5, … 8	
r_{out}	Active outer radius	150, 175, 200	mm
k_{HSBI}	HSR back iron thickness coefficient	0.4, 0.5, 0.6	
T_{HSPM}	HSR magnet thickness	3, 5, 7, … 13	mm
T_{AG}	Common air gap thickness	1.5	mm
T_{Mods}	Modulator thickness	11, 14, 17	mm
k_{PM}	LSR magnet thickness ratio	0.5, 0.75, 1	
T_{LSBI}	LSR back iron thickness	20, 25, 30	mm

Due to strong interdependencies between the effects of different dimensions, the values of certain variables were coupled through derived parameters, which are included in Table IV. As in [1], the radial thickness of the LSR magnets, T_{LSPM}, is determined by the radial thickness of the HSR magnets, T_{HSPM}, and a derived parameter, k_{PM}, according to

$$T_{LSPM} = k_{PM} T_{HSPM} . \tag{8}$$

Additionally, the HSR back iron thickness, T_{HSBI}, was sized based on the HSR permanent magnet pole arc and the derived scaler parameter, k_{HSBI}, according to

$$T_{HSBI} = k_{HSBI} \left(\pi r_{HSBI} / P_{HS} \right) \tag{9}$$

where r_{HSBI} denotes the outer radius of the HSR back iron. The term k_{HSBI} represents the idealized ratio of the HSR permanent magnet flux density to the HSR back iron flux density, based on a simplified model of the magnetic flux paths in the HSR. Thus, the thickness of the HSR back iron is sized based on the HSR permanent magnet pole arc and k_{HSBI}, where a larger value of k_{HSBI} indicates a lower magnetic loading in the HSR back iron. While the necessary sizing of the HSR back iron is dominated by the HSR permanent magnet pole arc, that of the LSR back iron is impacted by the pole arcs of both the HSR and LSR permanent magnets. Furthermore, it is often ultimately dictated by practical mechanical construction considerations. Therefore, a simple set of direct fixed values were considered for the LSR back iron thickness in the parametric optimization study.

The graphs in Figs. 8-11 and the statistics in Table V summarize the optimization study results. The plots in Fig. 8 illustrate the MEC's accuracy, using both the fine and coarse mesh settings, over the entire parametric sweep space. Both MECs are fairly accurate over a wide range of volumetric torque densities (VTD). Fig. 8(a) indicates that the fine mesh MEC torque predictions generally match the corresponding FEA torque predictions within approximately ±1%. The few exceptions to this tight error bound are some of the designs with the minimum HSR pole pair count of 3 and the maximum outer radius of 200 mm, which results in the maximum HSR pole arc. The fine mesh MEC slightly overestimates the torque ratings of these few designs by as much as 3.2%

because it does not account for the deep saturation in the LSR back iron caused by the large HSR pole arc. Fig. 8(b) demonstrates that the coarse mesh MEC model torque predictions are also fairly accurate over the full parametric sweep space, but tend to be slightly lower, with errors ranging from approximately -5% to +1%. This is primarily a result of using a smaller *ALM*, which, as shown in the discretization impact analysis, biases some of the torque predictions towards lower values and inadvertently helps to cancel out the worst overestimates produced by the fine mesh MEC.

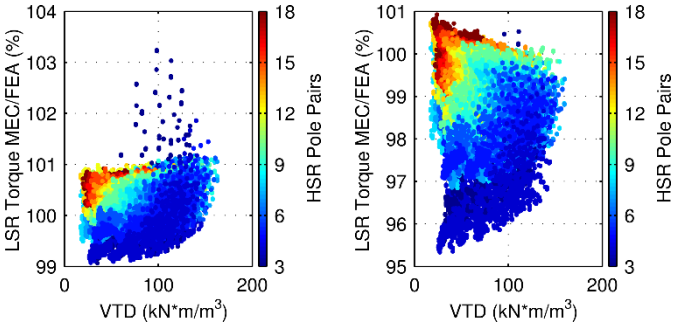

Fig. 8. MEC accuracy over the full parametric optimization sweep range using the (a) fine mesh and the (b) coarse mesh.

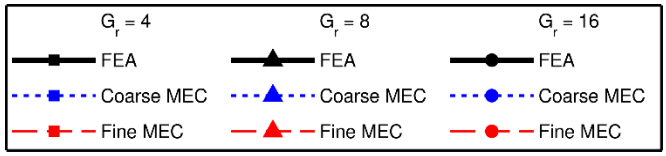

Fig. 9. Legend for design optimization trend plots in Figs. 10-11.

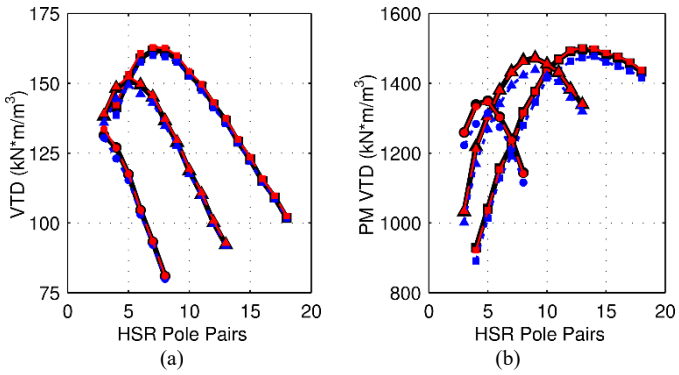

Fig. 10. Variation of the maximum achievable (a) volumetric torque density and (b) PM volumetric torque density with HSR pole pairs.

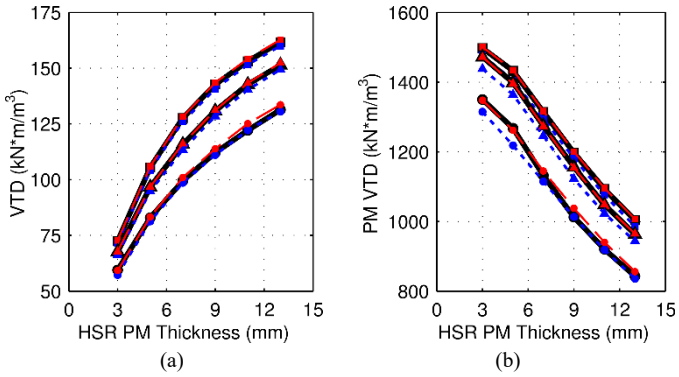

Fig. 11. Variation of the maximum achievable (a) volumetric torque density and (b) PM volumetric torque density with HSR PM thickness.

TABLE V
Summary of Optimization Study Results

Metric	Coarse Mesh MEC	Fine Mesh MEC	FEA
Minimum Percent Error	-4.7%	-0.9%	N/A
Maximum Percent Error	0.9%	3.2%	N/A
Average Percent Error	-1.2%	0.3%	N/A
Average Absolute Percent Error	1.3%	0.4%	N/A
Total Simulation Time (sec)	5078	31,492	1,390,599
Average Simulation Time (sec)	0.11	0.68	29.8

Fig. 9 provides a legend describing each curve in Figs. 10-11, which indicate optimization trends predicted by the FEA, coarse mesh MEC, and fine mesh MEC models for each of the three gear ratios considered in the study. In particular, Figs. 10-11 show the variation of two key design quality metrics, VTD and PM volumetric torque density (PM VTD), which is stall torque divided by PM material volume, with two of the most impactful design parameters, HSR pole pairs and HSR magnet thickness. VTD provides a normalized description of the size of each design. Optimization for VTD favors thicker magnets and lower pole counts. PM VTD characterizes the amount of magnet material required for each design and can serve as an approximate substitute for active material cost [1], which is dominated by the cost of the magnets. Optimization for PM VTD favors thinner magnets and higher pole counts. Figs. 10-11 demonstrate that both mesh settings provide very accurate characterizations of these different design trends.

Table V provides some statistics summarizing the accuracy and speed of the coarse and fine mesh MEC models relative to the FEA model over the entire parametric design space described in Table IV. These results and the information in Figs. 10-11 demonstrate that the MEC model is a very fast and accurate first pass analysis tool capable of tracking key design optimization trends. Although the fine mesh MEC model is slightly more accurate, the coarse mesh model is also fairly accurate and appreciably faster, which might make it a better option for use in some first pass analysis studies.

The MEC and FEA model simulation times depend on a plethora of considerations, including the designs evaluated and the computers used in the analysis. The timing statistics in Table V are simply intended to provide a general indication of the relative speeds of the different models, rather than an exact characterization. A strict convergence criteria of less than a 0.1% energy error and a minimum of 8 adaptive passes with a refinement rate of 30% per pass was used for the FEA model employed in this analysis to ensure extremely accurate results and a reliable set of reference data for comparison against the MEC model predictions. This convergence criteria results in final meshes consisting of 12,398, 10,222, and 9678 triangles for symmetric fractional FEA models of the three base designs described in Table I. Alternatively, the fine mesh symmetric fractional MEC models of the base designs, include 114,240, 63,840, and 157,560 nodes, while the coarse mesh symmetric fractional MEC models include 22,400, 13,300, and 29,640 nodes. Using a more typical, less strict FEA model convergence setting would yield comparable accuracy for

most (but not all) non-extreme design points and reduce the average simulation time to under 10 seconds per case. The average simulation time for both the MEC and FEA models was elevated due to the inclusion of high pole pair count designs, as increasing the pole count increases the requisite simulation time for both models. Regardless of these considerations, the study results indicate that the MEC model is exceptionally accurate and approximately 44-271 times faster than the FEA model. Some of this is attributed to the linearity of the MEC model and the fact that it predetermines the flux orientations in the flux tubes, while the FEA model is nonlinear and determines the flux orientation in each element as part of the solution. However, another factor is the MEC model's use of predetermined flux tube distributions which require negligible time to produce, as compared to the FEA model's adaptive mesh formation process. This suggests that a major difference in speeds between the two tools may not necessarily be an inherent difference between MEC and FEA models, but rather a result of these particular embodiments of the techniques. This ambiguity is a theme throughout MEC literature which frequently pits generalized commercial FEA software against custom MEC models that simply use fewer elements and produce less accurate solutions. However, these results clearly indicate that the MEC approach is an enticing and potentially situationally advantageous analysis technique.

VII. Conclusions

This is Part II of a two part paper on the development of a parameterized linear 2D MEC for radial flux magnetic gears with surface permanent magnets. Part I describes the systematic implementation of the MEC model. This section evaluates the MEC's performance and establishes its ability to quickly and accurately predict torque ratings and air gap flux densities for a wide range of designs. This study introduces several discretization parameters, analyzes their impact on simulation accuracy and speed, and derives more complex parameters which control the resolution in a given gear region based on its radial thickness and a pertinent pole arc length. These derived parameters facilitate efficient allocation of flux tubes for a wide range of designs without resulting in poor accuracy or excessively long simulation times. Finally, a 46,656 case parametric optimization study was conducted using both a coarse mesh MEC and a fine mesh MEC, which were 217 and 44 times faster than a nonlinear FEA model, while only exhibiting average errors of 1.26% and 0.39% relative to the FEA model's torque predictions. These exact results are a function of the study conditions, but they demonstrate that the MEC is much faster than a commercial FEA package and very accurate for most practical designs.

Future work on this subject will include the extension of the MEC model to three dimensions, the development of a non-linear MEC model variation using realistic ferromagnetic material B-H curve characteristics, and the application of the MEC model to other magnetic gear and machine topologies.

VIII. Acknowledgment

The authors would like to thank ANSYS for their generous support through the provision of FEA software.

IX. References

[1] M. Johnson, M. C. Gardner, and H. A. Toliyat, "Design Comparison of NdFeB and Ferrite Radial Flux Magnetic Gears," in *Proc. IEEE Energy Convers. Congr. and Expo.*, 2016, pp. 1-8.

[2] S. Gerber and R. J. Wang, "Analysis of the End-Effects in Magnetic Gears and Magnetically Geared Machines," in *Proc. Int. Conf. Elect. Mach.*, 2014, pp. 396-402.

[3] N. W. Frank and H. A. Toliyat, "Gearing Ratios of a Magnetic Gear for Wind Turbines," in *Proc. IEEE Int. Elect. Mach. and Drives Conf.*, 2009, pp. 1224-1230.

[4] T. Lubin, S. Mezani, and A. Rezzoug, "Analytical Computation of the Magnetic Field Distribution in a Magnetic Gear," *IEEE Trans. Magn.,* vol. 46, no. 7, pp. 2611-2621, Jul. 2010.

[5] T. Lubin, S. Mezani, and A. Rezzoug, "Development of a 2-D Analytical Model for the Electromagnetic Computation of Axial-Field Magnetic Gears," *IEEE Trans. Magn.,* vol. 49, no. 11, pp. 5507-5521, Nov. 2013.

[6] N. W. Frank, "Analysis of the Concentric Planetary Magnetic Gear," Ph.D. dissertation, Dept. Elect. and Comput. Eng., Texas A&M Univ., College Station, Tx., 2011.

[7] M. Fukuoka, K. Nakamura, and O. Ichinokura, "Dynamic Analysis of Planetary-Type Magnetic Gear Based on Reluctance Network Analysis," *IEEE Trans. Magn.,* vol. 47, no. 10, pp. 2414-2417, Oct. 2011.

[8] M. Fukuoka, K. Nakamura, and O. Ichinokura, "A Method for Optimizing the Design of SPM Type Magnetic Gear Based on Reluctance Network Analysis," in *Proc. Int. Conf. Elect. Mach.*, 2012, pp. 30-35.

[9] D. Thyroff, S. Meier, and I. Hahn, "Modeling Integrated Magnetic Gears Using a Magnetic Equivalent Circuit," in *Proc. Annu. Conf. IEEE Ind. Electron. Soc.*, 2015, pp. 2904-2908.

[10] R. C. Holehouse, K. Atallah, and J. Wang, "A Linear Magnetic Gear," in *Proc. Int. Conf. Elect. Mach.*, 2012, pp. 563-569.

X. Biographies

Matthew Johnson (S' 13, M'17) earned his B.S. in electrical engineering with a minor in mathematics from Texas A&M University, College Station, Texas in 2011. In 2017, he received a Ph.D. in electrical engineering while working in the Advanced Electric Machines and Power Electronics Laboratory at Texas A&M University. His research interests include magnetic gears, magnetically geared machines, and motor drives.

Matthew C. Gardner (S' 15) earned his B.S. in electrical engineering with a minor in Computer Science from Baylor University, Waco, Texas in 2014. He is currently pursuing a Ph.D. in electrical engineering while working in the Advanced Electric Machines and Power Electronics Laboratory at Texas A&M University. His research interests include optimal design and control of magnetic gears and magnetically geared machines.

Hamid A. Toliyat (S'87, M'91, SM'96, F'08) received the B.S, degree from Sharif University of Technology, Tehran, Iran in 1982, the M.S. degree from West Virginia University, Morgantown, WV in 1986, and the Ph.D. degree from University of Wisconsin-Madison, Madison, WI in 1991, all in electrical engineering. Following receipt of the Ph.D. degree, he joined the faculty of Ferdowsi University of Mashhad, Mashhad, Iran as an Assistant Professor of Electrical Engineering. In March 1994 he joined the Department of Electrical and Computer Engineering, Texas A&M University where he is currently the Raytheon endowed professor of electrical engineering. Dr. Toliyat has many papers and awards to his name, including the Nikola Tesla Field Award.